Granular Matter (2022) 24:36
https://doi.org/10.1007/s10035-021-01197-0

ORIGINAL PAPER

Assessing the wall effects of packed concentric cylinders and angular walls on granular bed porosity

Peter Michael Bandelt Riess[1] · Heiko Briesen[1] · Daniel Schiochet Nasato[1]

Received: 26 August 2021 / Accepted: 2 December 2021 / Published online: 7 January 2022

Abstract

The effect of added wall support on granular bed porosity is systematically studied to elucidate performance enhancements in filtration processes achieved by using inserts, as demonstrated experimentally (Bandelt Riess et al. in Chem Eng Technol 2018, 2021). Packed beds of spheres are simulated through discrete element method in cylinders with different internal wall configurations. Three containing systems are generated: concentric cylinders, angular walls, and a combination of both. Variations of particle size and wall friction and thickness are also considered, and the resulting granular bed porosities are analyzed. The porosity increase is proportional to the incorporated wall support; the combination of cylindrical and angular inserts displays the greatest effect (up to 26% increase). The sinusoidal porosity values near the walls are exhibited to clarify the effects. The presented method can change and evaluate granular bed porosity increments, which could lead to filtration process improvements, and the obtained behaviors and profiles can be used to explore additional effects and further systems.

Keywords Porosity · Wall support · Filter cake · Packed bed · DEM

List of symbols

Roman symbols

a	Empirical coefficient (–)
c	Viscous term (Ns m^{-1})
d	Sphere diameter (m)
D	Container diameter (m)
e	Coefficient of restitution (–)
F	Force (N)
g	Pair correlation function (–)
G	Shear modulus (Pa)
k	Elastic term (N m^{-1})
m	Particle mass (kg)
n	Particle number in a defined volume (–)
r	Particle position (m)
R	Particle radius (m)
Y	Young's modulus (Pa

Greek letters

β	Dissipative term (–)
Δ	Difference (–)
ε	Porosity (–)
μ_s	Coefficient of friction (–)
ν	Poisson's ratio (–)
ξ	Particle overlap (m)
ρ	Particle number density (m^{-3}

Subscripts

b	Bulk property
i	Particle name
j	Particle name
n	In normal direction
t	In tangential direction
∞	Located at the container center

Superscripts

^	Modifies e to unit vector
*	Equivalent property
′	Modifies D to distance between adjacent walls

Abbreviations

DEM	Discrete element method
RDF	Radial distribution function

✉ Daniel Schiochet Nasato
daniel.nasato@tum.de

[1] Chair of Process Systems Engineering, Technical University of Munich, TUM School of Life Sciences Weihenstephan, Gregor-Mendel-Str. 4, 85354 Freising, Germany

1 Introduction

Mechanical solid–liquid separation processes rely on physical principles to achieve their goal. The cake filtration process offers the advantage of allowing multiple applications, where the collected solids can be directly post-treated. During cake filtration, solid particles form porous, permeable layers with millimeters up to decimeters of thickness [1]. Porosity has a key role in filtration; hence, it has been thoroughly described by Tiller and co-workers in their notable works [2–4]. If solids are compressible, filter cake porosity is reduced in the direction of the filter medium, where the weight of all layers is supported, often leading to complications during equipment operation. Conversely, friction at the filter walls is known to consume part of the applied load, which should counteract compression. These two phenomena occur simultaneously during the process and can, therefore, be fruitfully set against each other [5]. Thus, adding more wall support through some random or structured packing should reduce filter cake compressibility, increasing porosity and throughput.

The common use of such packings is in absorption and rectification columns to increase the contact surface between phases as much as possible. Heat and mass transfers are enhanced, and equipment performs more effectively as a result. At the same time, they pose the benefit of exhibiting relatively low hydraulic pressure drops through the apparatus [6]. For these reasons, packings are a current topic in many investigations [7–10]. Furthermore, the effects of column walls on packed bed porosity are mentioned in various experimental and numerical works [11–15], allowing for an evident parallel to cake filtration.

The azimuthally averaged porosity of a granular medium (e.g., filter cake) contained in a cylinder changes with the radial position. If the solid particles are considered as randomly packed, uniform spheres, considerable amounts of data gathered in well-known works, such as those by Sonntag [16] and Jeschar [17], become available. Bulk porosity ε_b correlations are found in the following form:

$$\varepsilon_b = \varepsilon_\infty + a\frac{d}{D}, \tag{1}$$

where ε_∞ is the center porosity (no wall influence); a is an empirical coefficient; d is the sphere diameter; D is the container diameter. For monodisperse spheres poured into the column, Jeschar [17] reported bulk porosities between 0.375 and 0.391. Later, Desmond and Weeks [18] realized the importance of studying polydisperse packings because of the tendency of monodisperse ones to crystallize near flat walls.

More recently, Mueller [19] compiled the abovementioned works and several others as bases to improve existing models for predicting bulk and even local, radial porosities in a cylindrical bed of spheres, where the highest possible value (1) is always found at the container wall. However, studies regarding the strategic incorporation of more wall support and applications thereof are still scarce. This is understandable in the case of fixed beds for absorption and rectification, where wall effects are disadvantageous, causing channeling and reducing liquid residence time.

Nevertheless, using packed beds to incorporate more wall effects into separation processes involving solids retention has yielded promising results. This was approached in the case of high-performance liquid chromatography in Lan et al. [20] and Lan [21]. They investigated the enhancement of wall support inside a chromatography column packed with compressible materials by using different cylindrical insert configurations. Consequently, the compressible resins could endure a significantly higher throughput velocity at the onset compression. The results were a function of insert position, number, and dimensions, mechanical properties of the resins, and wall roughness.

In the field of cake filtration, Bandelt Riess et al. [5, 22] investigated similar phenomena using random and structured packings. Their effect was proposed as twofold: (1) a stationary effect, which, like a filter aid, provides a permeable structure with high porosity for the cake to accumulate; and (2) a transient effect, with which the packing's internal wall support counteracts the developing filter cake compression. Even though the transient effect was recently addressed in more detail [5], mechanistic explanations for the stationary one are still missing, which is the motivation of this study. To this end, numerical simulations based on discrete element method (DEM) have been identified as a useful tool for taking this systematic approach.

Modeling granular assemblies numerically employing discrete elements has been around for some time [23]. Nowadays, it can be applied to much more complex problems, such as studying the rearrangements of non-spherical particles through vibrations [24]. The investigation of porous media has benefited from the DEM simulations of, for example, Reboul et al. [25], who focused on the void size distribution of a packed bed, and Dong et al. [26], who focused on the influence of different forces on particles while sedimenting and forming filter cakes. More recently, Zhang and McCarthy [27] proposed a modified modeling approach for cake filtration by implementing a DEM-coupled method and comparing it with the classic Kozeny–Carman model [28]. The modified model more accurately predicted the flow rates in the case of polydisperse systems. McCarthy et al. [29] and Lovregio et al.

[30] showed that porosity values of spheres confined in annular and cylindrical cells, respectively, obtained through DEM and experimental methods can agree well quantitatively. Meanwhile, Gerontas et al. [31] successfully developed a structural mechanics model of resin compression in a liquid chromatography column, which used the finite element method to simulate the effect of wall support inside the column on the process in agreement with the experimental data of Lan et al. [20]. This consequently allowed the model to predict previously untested scenarios, thereby providing a convenient case study method.

This work aims at elucidating how wall support manipulation increases granular bed porosity in different scenarios. Different insert configurations are simulated to modify the porosity of cylindrical beds of uniform spheres. It is proposed that an insert geometry can be found, which provides significant porosity and permeability enhancements. This would support previous experimental results [22] and could lead to improvements in industrial filtration processes.

2 Methodology

2.1 Simulation method

LIGGGHTS software (Version 3.8.0; DCS Computing GmbH) was used to perform the numerical DEM simulations, while OVITO software (Version 3.0; OVITO GmbH) was utilized to visualize and calculate the radial distribution function (RDF). The RDF [also called pair correlation function $g(r)$] measures the probability of finding a particle at a distance r away from an arbitrary reference particle. It gives insight into the structure of the granular packing and is essentially a histogram of inter-particle distances. The RDF is given by [32]:

$$g(r) = \frac{n(r)}{4\pi r^2 \Delta r \rho^2}, \tag{2}$$

where $n(r)$ is the number of particles inside a spherical shell located between the radial distances r and $r + \Delta r$ from the center of the specified particle, and ρ is the number density of particles, that is, the total number of particles divided by the simulation cell volume [33]. The averaging is done over all particles in the system.

In the DEM, Newton's equations of motion are solved for the translational and rotational movements of all particles in the system. Particles do not deform during collisions but are allowed to overlap slightly instead. This overlap is given in normal direction as follows:

$$\xi_n = (R_i + R_j - \left|\vec{r}_i - \vec{r}_j\right|)\hat{e}_n, \tag{3}$$

where R_i, R_j, $\vec{r}_i$, and $\vec{r}_j$ are the radii and positions of particles i and j, respectively. The unit vector $\hat{e}_n$ is obtained from:

$$\hat{e}_n = \frac{\vec{r}_i - \vec{r}_j}{\left|\vec{r}_i - \vec{r}_j\right|}. \tag{4}$$

The contact force $\vec{F}$ between colliding particles is obtained from the Hertz [34] contact law in the normal direction and the model proposed by Mindlin and Deresiewicz [35] in the tangential direction. This contact force can be divided into a normal and a tangential component as:

$$\vec{F} = \vec{F}_n + \vec{F}_t \tag{5}$$

$$\vec{F}_n = \left(\vec{F} \cdot \hat{e}_n\right) = k_n \xi_n + c_n \dot{\xi}_n \tag{6}$$

$$\vec{F}_t = \vec{F} - \vec{F}_n = k_t \xi_t + c_t \dot{\xi}_t, \tag{7}$$

where k_n and k_t are the normal and tangential elastic terms, respectively, and c_n and c_t are the normal and tangential viscous terms, respectively. The equivalent mass m^* is calculated from the masses of particles i and j, denoted by m_i and m_j, respectively, following the rule below:

$$\frac{1}{m^*} = \frac{1}{m_i} + \frac{1}{m_j} \tag{8}$$

The elastic and viscous terms are given as follows, respectively:

$$k_n = \frac{4}{3} Y^* \sqrt{R^* \xi_n} \tag{9}$$

$$c_n = -\beta \sqrt{5 m^* k_n} \geq 0 \tag{10}$$

$$k_t = 8 G^* \sqrt{R^* \xi_n} \tag{11}$$

$$c_t = -\beta \sqrt{\frac{10}{3} m^* k_t} \geq 0, \tag{12}$$

where R^* is the equivalent radius calculated analog to Eq. (8). The parameter β is obtained from:

$$\beta = \frac{\ln(e)}{\sqrt{\ln^2(e) + \pi^2}}, \tag{13}$$

where e is the coefficient of restitution; Y^* is the equivalent Young's modulus obtained from Eq. (14); and G^* is the equivalent shear modulus obtained from Eq. (15).

$$\frac{1}{Y^*} = \frac{1-\nu_i^2}{Y_i} + \frac{1-\nu_j^2}{Y_j} \tag{14}$$

$$\frac{1}{G^*} = \frac{1-\nu_i^2}{G_i} + \frac{1-\nu_j^2}{G_j} \tag{15}$$

The coefficient of friction μ_s is defined as the upper limit of the tangential force through the Coulomb criterion:

$$F_t = \mu_s F_n. \tag{16}$$

The tangential damping contribution is only added in time steps without slip (i.e., the Coulomb criterion is not met). Please refer to Di Renzo and Di Maio [36] and Antypov [37] for a more detailed description.

The porosities were calculated using a Monte Carlo integration scheme (see Fig. 1), where 10^7 points were randomly seeded in the region of interest (annular region in this case). Increasing the number of points would have only yielded variations in the fourth decimal. For every generated point, it was checked if that point was inside of any of the spheres confined in the simulation's domain. The solid fraction in the region of interest was obtained from the ratio between the number of points inside spheres to the total number of randomly generated points. Accordingly, the void fraction was calculated as 1 minus the solid fraction. To avoid distortions in the results, the top layer of the particles was leveled according to the height of the lowest annular region. Particles above the aforementioned level were excluded from porosity calculations.

2.2 Simulation procedure

To validate the numerical simulations, the results were compared with the experimental data of Lovregio et al. [30] and Sederman et al. [38], as well as with the correlations of Sonntag [16], Jeschar [17], and De Klerk [39]. The procedure consisted of pouring monodisperse spheres inside a fixed-diameter cylinder and then calculating the bulk porosity. The coefficient of friction for the DEM simulations was initially calibrated until the simulation results matched one experimental point. Subsequently, further experimental and correlation data were simulated using the same coefficient of friction obtained from the calibration.

A cylinder with 22 mm diameter and monodisperse polypropylene spheres with 2.1, 3, 4, 5, and 6 mm diameters were used for the comparison with Lovregio et al. [30]. A cylinder with 45 mm diameter and monodisperse glass spheres of 3.2, 5, 7.5, 11.25, 15, and 22.5 mm diameters were used for the comparison with Sederman et al. [38].

The DEM model validated through Sederman et al. [38] was chosen to simulate the deposition of 3 mm diameter monodisperse spheres in newly defined systems. Additionally, slightly polydisperse particles with sizes ranging from 2.5 to 3.5 mm (3 mm average diameter) were used in further cases. Their size distribution was generated as follows: 10% of the bed mass consisted of particles with 2.5 cm diameter, 20% with 2.75 cm, 40% with 3.0 cm, 20% with 3.25 cm, and 10% with 3.5 cm. Using polydisperse particles allowed to avoid ordered arrangements as opposed to monodisperse ones. Seven systems were simulated:

(a) Concentric cylinders inserted into the 120 mm-diameter main cylinder: one to seven cylinders were inserted sequentially into the main cylinder, keeping a constant distance between adjacent cylinder walls. Figure 2 (top) depicts the cases with three and six internal cylinders. The walls were defined without thickness here to reduce variables and simplify the comparisons to the base case.
(b) Same setup as in (a) but using polydisperse particles.
(c) Same setup as in (b) but using a higher particle–wall coefficient of friction.

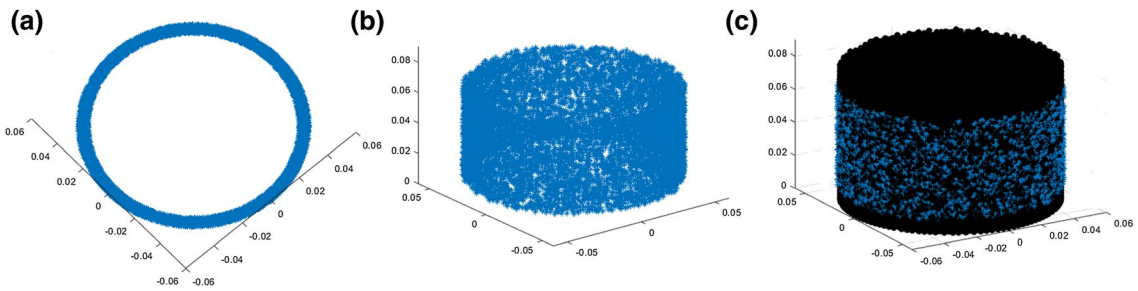

Fig. 1 Schematic of the Monte Carlo scheme implemented to calculate the void fraction. Points are randomly generated in the annular region of interest. **a** Is a top view and **b** is a side view of the generated points. The location of every point is checked against the position of all spheres in the simulation, as shown in **c**. The fraction of points inside spheres to the total number of points results in the solid fraction of the region of interest. The void fraction is obtained directly from the calculated solid fraction

(d) Same setup as in (a) but using 1 mm thick walls. Figure 2 (bottom) depicts the cases with three and six internal cylinders.
(e) Same setup as in (b) but using 1 mm thick walls.
(f) Angular walls inserted into the main cylinder: for this system, 4, 8, and 16 walls were used, keeping a constant angular distance between the walls. Polydisperse particles were used.
(g) Combination of systems (b) and (f): both concentric cylinders and angular walls were inserted into the main cylinder. Polydisperse particles were used. Figure 3 illustrates examples of systems (f) and (g).

The number of particles generated in each simulation varied depending on the particle size distribution, as well as on the number and thickness of the walls. The number of particles ranged from 37,404 to 43,500 in the different systems.

3 Results and discussion

3.1 Numerical validation

The parameter values used in the simulations for validation with the results of Lovregio et al. [30] and Sederman et al. [38] are shown in Table 1. The Poisson's ratio and coefficient of restitution for the comparison with Lovregio et al. [30] were the ones provided in the same study. The coefficient of friction was calibrated as described in the simulation procedure. For the comparison with Sederman et al. [38], the Poisson's ratio and coefficient of restitution were respectively obtained from Gu and Yang [40] and Tang et al. [41]. The walls were made of the same material as the particles, so the values in Table 1 were valid for the walls as well.

The obtained numerical results are compared with the experimental results of Lovregio et al. [30] and the correlations of De Klerk [39], Jeschar [17], and Sonntag [16] at defined D/d ratios in Table 2. A very good agreement is shown among the simulation, experimental, and correlation results for all the evaluated ratios. The largest discrepancy with the experimental results is 3.8%. The expected tendency of the porosity values to grow with decreasing D/d ratios is clear.

Table 3 shows the validation results against the experimental data of Sederman et al. [38]. A very good agreement is found between the simulations and the correlations for almost every investigated D/d ratio, except for the ratio of 3. This is attributed to the spheres forming an ordered arrangement in the simulation, as shown by evaluating its radial distribution function (Fig. 4).

The ordered arrangement formed by the spheres in Fig. 4a is characterized by the well-defined, isolated peaks of the RDF. Such regular arrangements produce denser sphere packings compared to irregular, amorphous ones [42]. As presented by Desmond and Weeks [18], monodisperse systems are susceptible to wall-induced crystallization, which modifies the structure of the granular bed near the walls, and this is confirmed here, justifying the need for further simulations with polydisperse particles. A continuous RDF without isolated peaks is shown for the amorphous structure is shown in Fig. 4b.

Having validated the simulation parameters and results, new systems and variations are introduced as noted in Sect. 2.2.

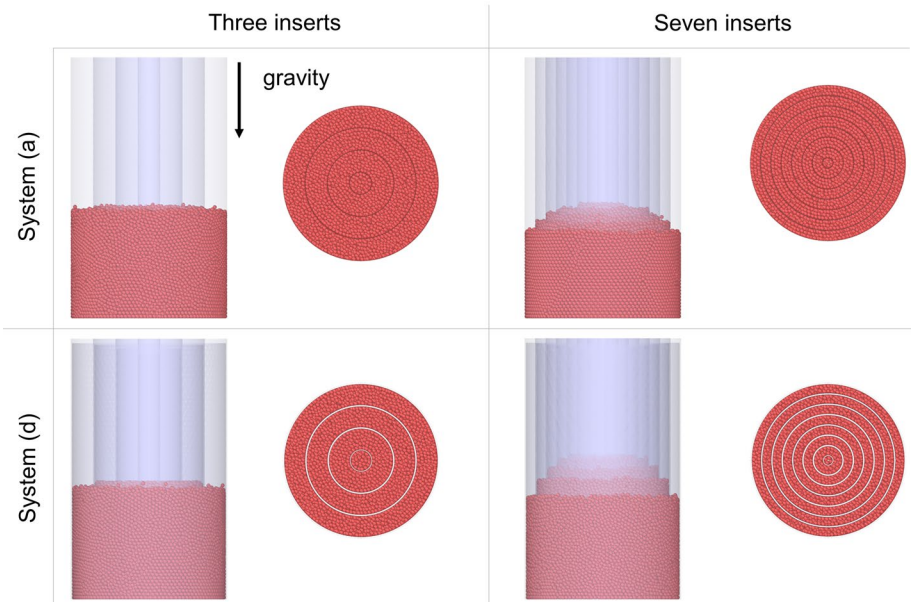

Fig. 2 Top: simulation setups of system (a) using three and seven inserts. Bottom: setups of system (d) using three and seven inserts

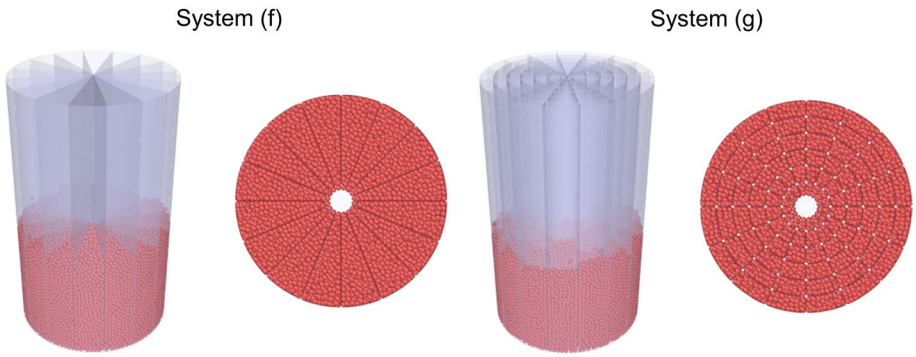

Fig. 3 Simulation setups of system (f) using 16 angular walls (left) and system (g) combining six inner cylinders with 16 angular walls (right)

Table 1 Parameter values used in the validations of the numerical simulations

Parameter	Validation with Lovregio et al. [30]	Validation with Sederman et al. [38]
Young's modulus	1×10^8 Pa	1×10^8 Pa
Poisson's ratio	0.42	0.23
Coefficient of friction	0.36	0.19
Coefficient of restitution	0.66	0.93

Table 2 Bulk porosity validation using the experimental data of Lovreglio and the correlations of De Klerk, Jeschar, and Sonntag

D/d	10.5	7	5.25	4.2	3.5
Simulation	0.403	0.423	0.443	0.452	0.491
Lovreglio (exp.)	–	0.410	0.440	0.470	–
De Klerk ($\varepsilon_\infty = 0.391$)	0.397	0.414	0.436	0.459	0.480
Jeschar ($\varepsilon_\infty = 0.375$)	0.407	0.424	0.439	0.456	0.472
Sonntag ($\varepsilon_\infty = 0.375$)	0.406	0.422	0.437	0.453	0.469

The ε_∞ values used for the correlations are also indicated

3.2 Numerical experiments

Systems (a)–(c) are discussed first. Table 4 shows the bulk porosities calculated in the main cylinder without inserts as a reference. The D/d ratio is maximal here and equal to 40. The mean porosity values were obtained from five measurements in different positions of the bed. The control region for porosity calculations was a cylinder with the diameter of the outer cylinder and a height of 30 mm. The respective standard deviations were also calculated. The number of inner cylinders was then incremented to up to seven inserts, where the D'/d ratio was equal to 2.67 in each annulus (D' being the shortest distance between adjacent walls). The insert diameters were previously selected such that all walls would be equidistant.

For system (a) containing monodisperse particles, the bulk porosity does not exhibit a very clear trend. An overall increase with insert number is observed. However, inserting four, five, and seven cylinders caused porosity decrements. This is due to the ordered arrangement of monodisperse particles, which is seen in Fig. 5. The structural arrangements in Fig. 5a, b are in sharp contrast. It is remarked that monodispersity is an idealization.

In opposition, the polydisperse systems (closer to reality) follow a clear trend. As shown in Fig. 5c, d such particles did not form ordered arrangements. The most noticeable porosity increase is by 15.5% (compared to the reference) from five to six inserts. These results do not correspond with the correlations for cylindrically packed beds, which predict porosity increases of over 20% for a D/d of 4 and over 30% for a D/d of 3. Nevertheless, a direct transference cannot be made here because additional effects appear in these systems due to the internal

Table 3 Bulk porosity validation using the experimental data of Sederman and the correlations of De Klerk, Jeschar, and Sonntag

D/d	14	9	6	4	3	2
Simulation	0.384	0.400	0.415	0.432	0.431	0.531
Sederman (exp.)	0.385	0.400	–	–	–	–
De Klerk ($\varepsilon_\infty = 0.391$)	0.392	0.401	0.425	0.465	0.500	0.551
Jeschar ($\varepsilon_\infty = 0.375$)	0.399	0.413	0.432	0.460	0.488	0.545
Sonntag ($\varepsilon_\infty = 0.375$)	0.398	0.412	0.430	0.457	0.485	0.540
Sonntag ($\varepsilon_\infty = 0.359$)	0.383	0.396	0.415	0.443	0.471	0.527

The ε_∞ values used for the correlations are also indicated

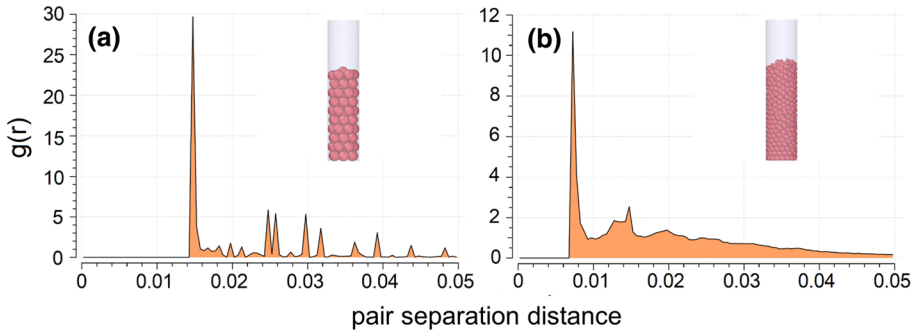

Fig. 4 Radial distribution function calculated for the D/d ratios **a** 3 and **b** 6

Table 4 ε_b Values for different numbers of volume-less cylindrical inserts

Insert number	D'/d	ε_b (a)	ε_b (b)	ε_b (c)
0	40	0.367 ± 0.008	0.367 ± 0.007	0.367 ± 0.007
1	13.33	0.372 ± 0.004	0.371 ± 0.003	0.372 ± 0.002
2	8	0.380 ± 0.002	0.379 ± 0.001	0.381 ± 0.001
3	5.71	0.391 ± 0.004	0.389 ± 0.001	0.390 ± 0.000
4	4.44	0.380 ± 0.002	0.395 ± 0.001	0.398 ± 0.001
5	3.64	0.376 ± 0.002	0.403 ± 0.001	0.406 ± 0.000
6	3.08	0.428 ± 0.001	0.423 ± 0.001	0.425 ± 0.001
7	2.67	0.409 ± 0.009	0.422 ± 0.003	0.425 ± 0.001

walls (it is not a reduction but a division). To the best of the authors' knowledge, these correlations have not yet been investigated. However, they show potential considering that merely the right number of inserts can cause the observed effects, which would considerably increase a packed bed's permeability.

Table 4 also shows that a seventh insert did not affect the bulk porosities. Effects similar to the one for the monodisperse case may have taken place. However, ordered arrangements could not be identified (see Fig. 5d).

When the friction between particles and walls was increased from 0.19 to 0.9 [system (c)], there were no changes in bulk porosity in comparison with system (b). This indicates that the frictional forces at the walls are dissipated in the granular material, probably due to the large granular arrangement in the azimuthal direction between the cylinders. Therefore, very specific wall material properties would not be necessary to obtain such porosity increases in a rigid granular bed. Nevertheless, this would likely play a role in a highly compressible one, as seen in Bandelt Riess et al. [5].

Systems (d) and (e) evaluate the insertion of cylinders with 1 mm thickness and the results are shown in Table 5. Note that the D'/d ratios are different from those in the previous cases. The porosities of system (d) follow a clearer trend than that of system (a), and porosity was greatly increased by 26% with the seventh insert. System (e) exhibits a very similar trend, and the obtained values are comparable to those of system (b). This would mean that the porosity increases are mainly a function of D'/d with wall thickness becoming a rather secondary variable. Both systems (d) and (e) show noticeable deviations from the observed tendencies when using six inserts, which can again be attributed to ordered arrangements.

The results of systems (b) and (e) were modeled by fitting an equation in the form of the correlation of De Klerk [39] for the region of interest. Figure 6 depicts the fitted curve and the equation parameters. D'/d values up to 8 were used to fit the curve since larger values caused only small porosity increments. Results altered by ordered arrangements were not considered for the fitting. The coefficient of determination (R^2) for the fitted curve is 0.97.

Note that only bulk porosities of entire systems have been discussed so far. Despite all adjacent cylinder walls being equidistant, the porosity is mostly increased in the central cylinder. This is due to the differences in geometry and wall distribution between the inner cylindrical region and outer annular regions. Figure 7 shows the porosity values inside each annulus for system (b) using different numbers of inserts. The porosity in the innermost region, which is purely cylindrical, follows the correlations of De Klerk or

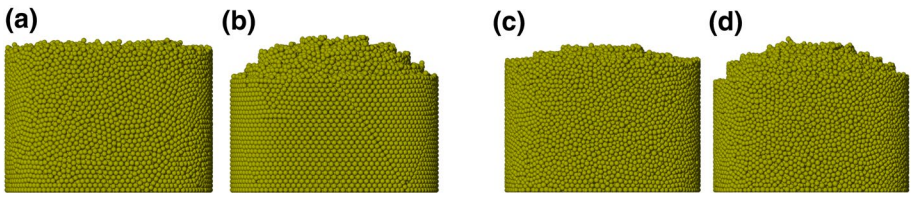

Fig. 5 Monodisperse particles with **a** three and **b** seven inserts. Polydisperse particles with **c** three and **d** seven inserts

Jeschar. This result is thus attributed to a higher amount of particle–wall contact points and points towards equipment designs maximizing it. However, the annular regions of the system exhibit a lower porosity than predicted, which behaves as a constant. In a separation process, this could ensure a homogeneous porosity distribution in the filter cake and become a great advantage.

The porosity results are also analyzed as a function of distance from the outer cylinder wall. The obtained values display the classical sinusoidal behavior in all cases. Near the walls, the particles inefficiently pack into layers (particle density heterogeneity) and cause the observed porosity oscillations and packing behavior changes [18]. The peak porosity values (nearly 1) mark the particle–wall contact region where the inner cylinders were inserted, thereby contributing positively to the bulk porosity. In the reference case, the layering influence covers about two particle diameters and decays into the bulk for ten diameters. Figure 8 shows the results for the reference, three, and six inner cylinders.

Angular walls were inserted to change the bulk porosity in system (f). In addition to angular walls, three and six inner cylinders were again inserted into system (g). Table 6 presents the obtained results. For some geometries, the innermost region had to be removed from the calculations because they became too small for the spheres to enter. Nevertheless, the bulk porosities increase remarkably compared to system (b). This happens not only for a constant number of cylinders and a growing angular wall number but also for a constant angular wall number and a growing cylinder number. That is, the more walls there are, the greater is the effect, leading to up to a 26% porosity increase, which would cause a corresponding permeability enhancement. Figure 9 illustrates the porosity profile of system (f).

The sinusoidal profile is well captured near the wall (at $D/d = 40$) and similar for all studied cases. At this point, the angular walls are furthest away from each other and do not affect the porosity significantly. In contrast, their wall effects become clear near the center region of the system. In particular, for the 8 and 16 inserts, the porosity is increased

Table 5 ε_b Values for different numbers of 1 mm thick cylindrical inserts

Insert number	D'/d	ε_b (d)	ε_b (e)
0	39.33	0.368 ± 0.009	0.368 ± 0.008
1	13	0.373 ± 0.005	0.372 ± 0.002
2	7.67	0.381 ± 0.002	0.381 ± 0.001
3	5.38	0.386 ± 0.002	0.390 ± 0.000
4	4.11	0.406 ± 0.000	0.402 ± 0.000
5	3.30	0.419 ± 0.000	0.415 ± 0.001
6	2.74	0.380 ± 0.003	0.415 ± 0.001
7	2.33	0.464 ± 0.000	0.454 ± 0.001

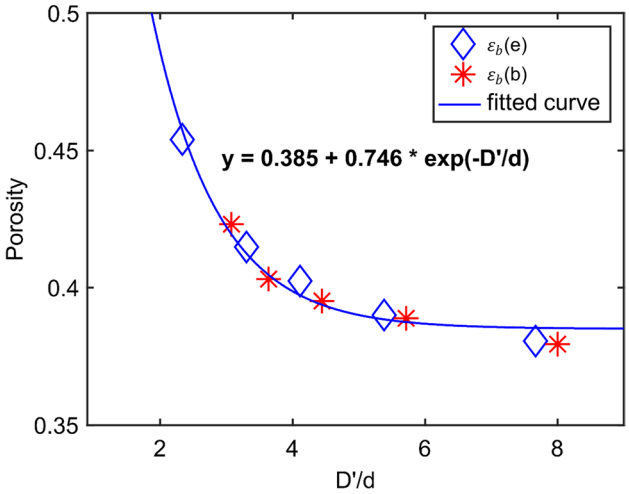

Fig. 6 Equation fitted to the numerical bulk porosity results of systems (b) and (e)

to 1 before reaching the middle, revealing the region where the spheres do not fit anymore.

Figures 10 and 11 show the obtained porosity profiles for system (g), which contained three and six inner cylinders in addition to the 4, 8, and 16 angular walls, respectively. The sinusoidal profile is again well captured near the wall and similar for all studied cases, regardless of the cylinder number. Another property of these cases is the symmetrical evolution of the porosity value between the walls. The porosity again increases to 1 near the center because no particles could be deposited in that region. The interference of the angular walls is noticeable upon reaching that point, further increasing the overall porosity (Table 6).

Considering the presented cases, it becomes clearer how particles interact with different packed wall configurations, increasing bed porosity and therefore permeability as well.

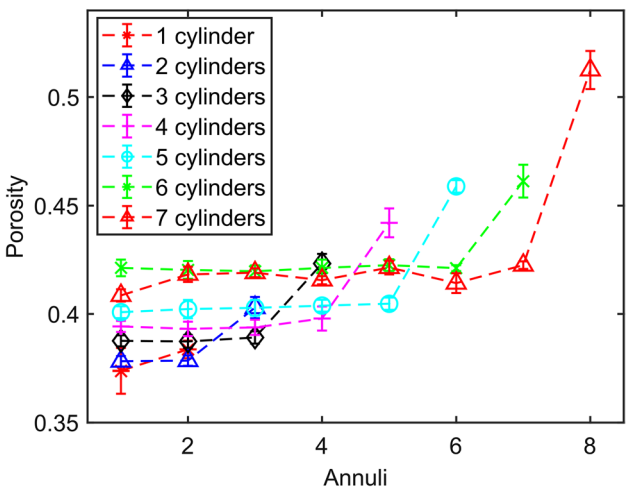

Fig. 7 Porosity calculated in the different annuli of system (b)

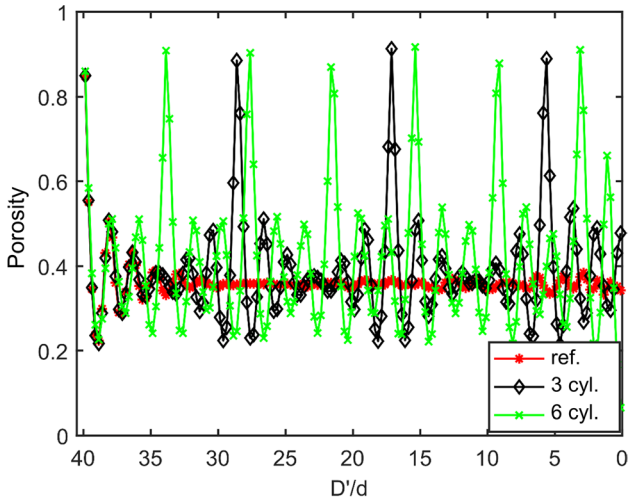

Fig. 8 Porosity of system (b) as a function of distance from the outer wall for the reference and with three and six inner cylinders

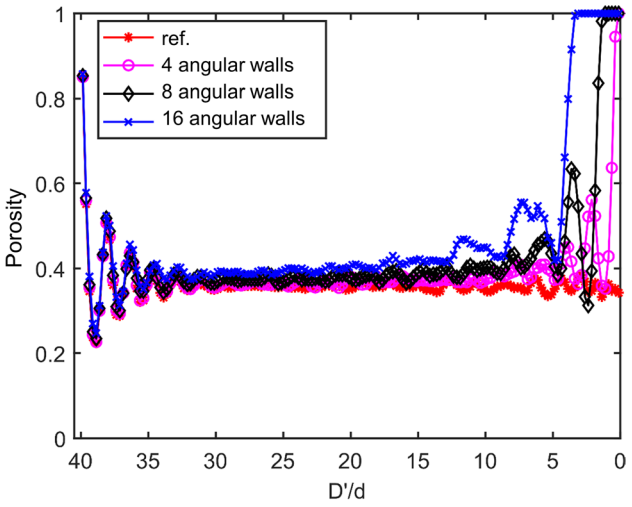

Fig. 9 Porosity of system (f) as a function of the distance from the outer wall for the insertion of 0, 4, 8, and 16 angular walls

This would contribute to the flow velocity in a solid–liquid separation through a structured packing and explain part of the effects observed by Bandelt Riess et al. [22]. Moreover, the obtained behaviors and profiles can be used to explore further systems and additional effects.

4 Conclusions and outlook

This investigation demonstrated how using different packed wall configurations affects the porosity of a granular bed. The DEM simulations were set up and validated with literature data. Ordered arrangements were observed in the monodisperse systems (as was expected, considering the literature), which cannot be predicted with the correlations of Sonntag [16], Jeschar [17], and De Klerk [39] (Table 3).

Adding inner concentric cylinders, angssular inserts, or a combination of both generally increased the bulk porosity due to the wall effects. They favorably reproduced the known sinusoidal porosity profile, which is commonly observed only in the near-wall region of the outer cylinder. Since the comparison to usual porosity correlations for granular beds confined in cylindrical containers was limited by the newly evaluated geometries, a new specific correlation was defined.

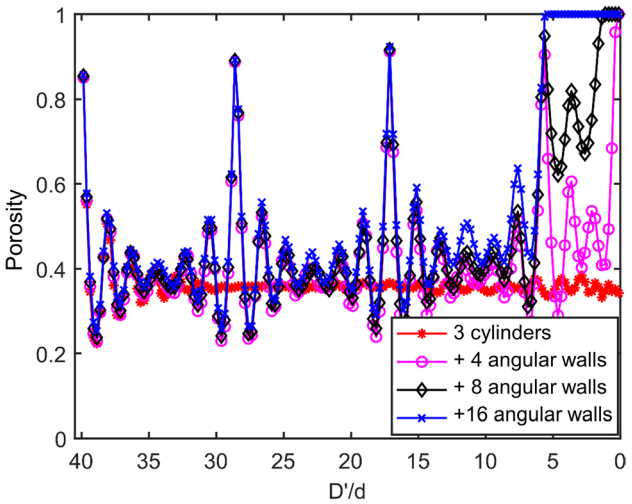

Fig. 10 Porosity of system (g) as a function of the distance from the outer wall for the insertion of 3 cylinders and 0, 4, 8, and 16 angular walls

A distance between adjacent walls was found at six cylindrical inserts for system (b), which caused a significant porosity enhancement. This elucidates the geometric interactions needed to improve throughput in a filter cake.

Table 6 ε_b Values for the systems containing 0, 4, 8, and 16 angular walls combined with 0, 3, and 6 cylindrical inserts

Cylinder no	0 ($D'/d = 40$)				3 ($D'/d = 5.71$)				6 ($D'/d = 3.08$)			
Angular wall no	0	4	8	16	0	4	8	16	0	4	8	16
ε_b	0.367	0.378	0.389	0.410	0.389	0.400	0.413	0.429	0.423	0.435	0.444	0.462
Std. Dev	0.007	0.008	0.007	0.008	0.001	0.008	0.007	0.007	0.001	0.007	0.007	0.007

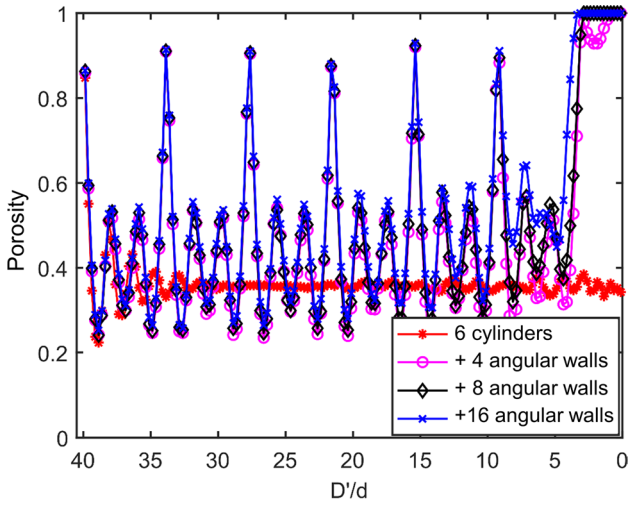

Fig. 11 Porosity of system (g) as a function of the distance from the outer wall for the insertion of 6 cylinders and 0, 4, 8, and 16 angular walls

Furthermore, a homogeneous porosity distribution was observed in the annular spaces of this system, showing potential for applications demanding porosity control, such as the freeze-drying of bulky solids [43] and heat transfer in a fixed-bed reactor [44].

Additionally, variations of the coefficient of friction and insert thickness were considered but did not show significant effects. Future work should involve applying the variations to highly compressible particles. Other studies could assume the task of rigorously optimizing insert number and placement for a given system and experimentally validating the predictions. Additional control variables of interest could be the pressure at the walls and the contact forces between particles.

Using angular walls [system (f)] had a mild effect on the granular bed. However, in combination with the inner cylinders [system (g)], the increase in the bulk porosity was remarkable (up to 26%), which could lead to significant improvements in solid–liquid separation processes. In these cases, the increasing size of the center region, where no particle can be inserted, must be considered.

System (g) can be roughly compared to the structures of a Raflux or Pall ring, which have already been experimentally tested [5, 22]. Future investigations should benefit from this research to find further numerical and practical correlations.

Authors' contributions Conceptualization: all authors; Data curation: Schiochet Nasato; Formal analysis: Bandelt Riess, Schiochet Nasato; Funding acquisition: Briesen; Investigation: Bandelt Riess, Schiochet Nasato; Methodology: Bandelt Riess, Schiochet Nasato; Project administration: all authors; Resources: Briesen; Software: Schiochet Nasato; Supervision: Briesen; Validation: Schiochet Nasato; Visualization: Bandelt Riess, Schiochet Nasato; Writing—original draft: Bandelt Riess, Schiochet Nasato; Writing—review & editing: all authors.

Funding Open Access funding enabled and organized by Projekt DEAL. This work was supported by the Research Association of the German Food Industry (FEI) via AiF (19359 N) within the program for promoting the Industrial Collective Research (IGF) of the German Ministry of Economic Affairs and Energy (BMWi).

Availability of data and material The datasets generated and analysed during the current study are available from the corresponding author on reasonable request.

Declarations

Conflicts of interest The authors have no relevant financial or non-financial interests to disclose.

References

1. Anlauf H (2020) Wet cake filtration. Fundamentals, equipment, strategies. WILEY VCH, Weinheim (2020)
2. Tiller, F.M., Haynes, S., Lu, W.-M.: The role of porosity in filtration VII effect of side-wall friction in compression-permeability cells. AIChE J. (1972). https://doi.org/10.1002/aic.690180104
3. Tiller, F.M., Green, T.C.: Role of porosity in filtration IX skin effect with highly compressible materials. AIChE J. (1973). https://doi.org/10.1002/aic.690190633
4. Tiller, F.M., Kwon, J.H.: Role of porosity in filtration: XIII. Behavior of highly compactible cakes. AIChE J. (1998). https://doi.org/10.1002/aic.690441005
5. Bandelt Riess, P.M., Kuhn, M., Först, P., Briesen, H.: Investigating the effect of packed structures on filter cake compressibility. Chem. Eng. Technol. (2021). https://doi.org/10.1002/ceat.202000451
6. Maćkowiak, J.: Fluiddynamik von Füllkörpern und Packungen. Springer, Berlin (2003)
7. Fee, C., Nawada, S., Dimartino, S.: 3D printed porous media columns with fine control of column packing morphology. J. Chromatogr. A (2014). https://doi.org/10.1016/j.chroma.2014.01.043
8. Nawada, S., Dimartino, S., Fee, C.: Dispersion behavior of 3D-printed columns with homogeneous microstructures comprising differing element shapes. Chem. Eng. Sci. (2017). https://doi.org/10.1016/j.ces.2017.02.012
9. Neukäufer, J., Hanusch, F., Kutscherauer, M., Rehfeldt, S., Klein, H., Grützner, T.: Methodik zur Entwicklung additiv gefertigter Packungsstrukturen im Bereich der thermischen Trenntechnik. Chem. Ing. Tech. (2019). https://doi.org/10.1002/cite.201800171

10. Marek, M., Niegodajew, P.: A new experimental approach to examination of orientation distribution of cylindrical particles in random packed beds. Powder Technol. (2020). https://doi.org/10.1016/j.powtec.2019.10.077
11. Cohen, Y., Metzner, A.B.: Wall effects in laminar flow of fluids through packed beds. AIChE J. (1981). https://doi.org/10.1002/aic.690270502
12. Bey, O., Eigenberger, G.: Fluid flow through catalyst filled tubes. Chem. Eng. Sci. (1997). https://doi.org/10.1016/S0009-2509(96)00509-X
13. Wang, Z., Afacan, A., Nandakumar, K., Chuang, K.T.: Porosity distribution in random packed columns by gamma ray tomography. Chem. Eng. Process. Process Intensif. (2001). https://doi.org/10.1016/S0255-2701(00)00108-2
14. Di Felice, R., Gibilaro, L.G.: Wall effects for the pressure drop in fixed beds. Chem. Eng. Sci. (2004). https://doi.org/10.1016/j.ces.2004.03.030
15. Allen, K.G., von Backström, T.W., Kröger, D.G.: Packed bed pressure drop dependence on particle shape, size distribution, packing arrangement and roughness. Powder Technol. (2013). https://doi.org/10.1016/j.powtec.2013.06.022
16. Sonntag, G.: Einfluß des Lückenvolumens auf den Druckverlust in gasdurchströmten Füllkörpersäulen. Chem. Ing. Tech. (1960). https://doi.org/10.1002/cite.330320502
17. Jeschar, R.: Druckverlust in Mehrkornschüttungen aus Kugeln. Arch. Eisenhüttenwes. (1964). https://doi.org/10.1002/srin.196402300
18. Desmond, K.W., Weeks, E.R.: Random close packing of disks and spheres in confined geometries. Phys. Rev. E Stat. Nonlinear Soft Matter Phys. (2009). https://doi.org/10.1103/PhysRevE.80.051305
19. Mueller, G.E.: A modified packed bed radial porosity correlation. Powder Technol. (2019). https://doi.org/10.1016/j.powtec.2018.10.030
20. Lan, T., Gerontas, S., Smith, G.R., Langdon, J., Ward, J.M., Titchener-Hooker, N.J.: Investigating the use of column inserts to achieve better chromatographic bed support. Biotechnol. Progr. (2012). https://doi.org/10.1002/btpr.1597
21. Lan, T.: An experimental and simulation study of the influence made by inserts on chromatographic packed bed hydrodynamics. Doctoral dissertation, London (2013)
22. Bandelt Riess, P.M., Engstle, J., Kuhn, M., Briesen, H., Först, P.: Decreasing filter cake resistance by using packing structures. Chem. Eng. Technol. (2018). https://doi.org/10.1002/ceat.201800254
23. Cundall, P.A., Strack, O.D.L.: A discrete numerical model for granular assemblies. Géotechnique (1979). https://doi.org/10.1680/geot.1979.29.1.47
24. Wu, Y., An, X., Yu, A.B.: DEM simulation of cubical particle packing under mechanical vibration. Powder Technol. (2017). https://doi.org/10.1016/j.powtec.2016.09.029
25. Reboul, N., Vincens, E., Cambou, B.: A statistical analysis of void size distribution in a simulated narrowly graded packing of spheres. Granul. Matter (2008). https://doi.org/10.1007/s10035-008-0111-5
26. Dong, K.J., Zou, R.P., Yang, R.Y., Yu, A.B., Roach, G.: DEM simulation of cake formation in sedimentation and filtration. Miner. Eng. (2009). https://doi.org/10.1016/j.mineng.2009.03.018
27. Zhang, S., McCarthy, J.J.: Modeling of the pressure drop across polydisperse packed beds in cake filtration. AIChE J. (2019). https://doi.org/10.1002/aic.16557
28. Bear, J.: Modeling phenomena of flow and transport in porous media. Theory and applications of transport in porous media, vol. 31. Springer, Cham (2018)
29. McCarthy, J.J., Jasti, V., Marinack, M., Higgs, C.F.: Quantitative validation of the discrete element method using an annular shear cell. Powder Technol. (2010). https://doi.org/10.1016/j.powtec.2010.04.011
30. Lovreglio, P., Das, S., Buist, K.A., Peters, E.A.J.F., Pel, L., Kuipers, J.A.M.: Experimental and numerical investigation of structure and hydrodynamics in packed beds of spherical particles. AIChE J. (2018). https://doi.org/10.1002/aic.16127
31. Gerontas, S., Lan, T., Micheletti, M., Titchener-Hooker, N.J.: Evaluation of a structural mechanics model to predict the effect of inserts in the bed support of chromatographic columns. Chem. Eng. Sci. (2015). https://doi.org/10.1016/j.ces.2015.02.010
32. Parafiniuk, P., Molenda, M., Horabik, J.: Influence of particle shape and sample width on uniaxial compression of assembly of prolate spheroids examined by discrete element method. Phys. A Stat. Mech. Appl. (2014). https://doi.org/10.1016/j.physa.2014.08.063
33. Stukowski, A.: Visualization and analysis of atomistic simulation data with OVITO–the Open Visualization Tool. Model. Simul. Mater. Sci. Eng. (2010). https://doi.org/10.1088/0965-0393/18/1/015012
34. Hertz, H.: Über die Berührung fester elastischer Körper. J. Reine. Angew. Math. **92**, 156–171 (1881)
35. Mindlin, R.D., Deresiewicz, H.: Elastic spheres in contact under varying oblique force. Trans. ASME J. Appl. Mech. **20**, 327–344 (1953)
36. Di Renzo, A., Di Maio, F.P.: Comparison of contact-force models for the simulation of collisions in DEM-based granular flow codes. Chem. Eng. Sci. (2004). https://doi.org/10.1016/j.ces.2003.09.037
37. Antypov, D., Elliott, J.A.: On an analytical solution for the damped Hertzian spring. EPL (2011). https://doi.org/10.1209/0295-5075/94/50004
38. Sederman, A.J., Alexander, P., Gladden, L.F.: Structure of packed beds probed by magnetic resonance imaging. Powder Technol. (2001). https://doi.org/10.1016/S0032-5910(00)00374-0
39. de Klerk, A.: Voidage variation in packed beds at small column to particle diameter ratio. AIChE J. (2003). https://doi.org/10.1002/aic.690490812
40. Gu, X.Q., Yang, J.: A discrete element analysis of elastic properties of granular materials. Granul. Matter (2013). https://doi.org/10.1007/s10035-013-0390-3
41. Tang, H., Song, R., Dong, Y., Song, X.: Measurement of restitution and friction coefficients for granular particles and discrete element simulation for the tests of glass beads. Materials (Basel, Switzerland) (2019). https://doi.org/10.3390/ma12193170
42. Hales, T.C.: Historical overview of the Kepler conjecture. Discret. Comput. Geom. (2006). https://doi.org/10.1007/s00454-005-1210-2
43. Foerst, P., Gruber, S., Schulz, M., Vorhauer, N., Tsotsas, E.: Characterization of Lyophilization of Frozen Bulky solids. Chem. Eng. Technol. (2020). https://doi.org/10.1002/ceat.201900500
44. Eppinger, T., Jurtz, N., Kraume, M.: Influence of macroscopic wall structures on the fluid flow and heat transfer in fixed bed reactors with small tube to particle diameter ratio. Processes (2021). https://doi.org/10.3390/pr9040689